Micro-Doppler based Recognition of Ballistic Targets using 2D Gabor Filters

Adriano Rosario Persico, Carmine Clemente, Christos V. Ilioudis,
Domenico Gaglione, Jianlin Cao and John Soraghan
*University of Strathclyde, CESIP, EEE, 204, George Street, G1 1XW, Glasgow, UK
E-mail: adriano.persico, carmine.clemente, c.ilioudis, domenico.gaglione, jianlin.cao, j.soraghan- @strath.ac.uk

***Abstract*—The capability to recognize ballistic threats, is a critical topic due to the increasing effectiveness of resultant objects and to economical constraints. In particular the ability to distinguish between warheads and decoys is crucial in order to mitigate the number of shots per hit and to maximize the ammunition capabilities. For this reason a reliable technique to classify warheads and decoys is required. In this paper the use of the micro-Doppler signatures in conjunction with the 2-Dimensional Gabor filter is presented for this problem. The effectiveness of the proposed approach is demonstrated through the use of real data.**

I. Introduction

The interest in recognition and classification of ballistic targets has grown in the last years. In particular, significant attention has been given to the challenge of distinguishing between warheads and decoys. The latter are objects of different shapes released by the missiles in order to introduce confusion in the interceptors. Since it is clear that warheads and decoys make specific micro-motions during their ballistic trajectory, the micro-Doppler effect analysis introduced in [1], and widely investigated in the last decade [2], may be used for the purpose of information extraction for target classification. Specifically, the warheads may be characterized by precession and nutation, while the decoys wobble, as described in [3] and [4]. Such different micro-motions generate different micro-Doppler signatures in the returned radar signal.

Classification based on the micro-Doppler signatures has been employed in [5] and [6] with feature extraction based on the Pseudo-Zernike moments.

In this paper, a novel algorithm for radar micro-Doppler classification based on the processing of the Cadence Velocity Diagram (CVD) with Gabor filter is presented. The Gabor filter has been successfully employed to extract reliable features in many different applications [7],[8],[9]. In particular, they have been usually used for texture and symbol classification, as in [7] and [10], and for face recognition in [11]. The scale, translation, rotation and illumination invariant properties of the filter have been utilised in these applications. The Gabor filter is capable of extracting local information from the micro-Doppler signature of the target of interest [12].

The remainder of the paper is organized as follows. Section II reviews the relevant 2D Gabor filter theory, while Section III describes the novel feature extraction algorithm. In Section IV the effectiveness of the proposed approach is demonstrated on real data. Section V concludes the paper.

II. Gabor Filter Global Feature

The 2D Gabor function is the product of a complex exponential representing a sinusoidal plane wave and an elliptical Gaussian in any rotation. The filter response in the continuous domain can be normalized to have a compact closed form [7],[11]

$$\psi(x,y) = \frac{f^2}{\pi\gamma\eta}\, e^{-\left(\frac{f^2}{\gamma^2}x'^2+\frac{f^2}{\eta^2}y'^2\right)} e^{j2\pi f x'} \tag{1}$$

with

$$x' = x\cos(\theta) + y\sin(\theta), \quad y' = -x\sin(\theta) + y\cos(\theta) \tag{2}$$

where f is the central spatial frequency of the filter, θ is the anti-clockwise rotation of the Gaussian envelope and the sinusoidal plane wave, γ is the spatial width of the filter along the plane wave, and η is the spatial width perpendicular to the wave. The sharpness of the filter is controlled on the major and the minor axes by η and γ, respectively, defining the aspect ratio of the Gaussian as $\lambda = \eta/\gamma$. The normalized filter harmonic response is [7]

$$\Psi(u,v) = e^{-\frac{\pi^2}{f^2}\left(\gamma^2\left(u'-f\right)^2+\eta^2 v'^2\right)} \tag{3}$$

where

$$u' = u\cos(\theta) + v\sin(\theta), \quad v' = -u\sin(\theta) + v\cos(\theta). \tag{4}$$

Figure 1 represents the real part of a Gabor filter response in the XY plane, with $\eta = \gamma = 2\pi$, $f = 4$ and for different orientation angles. In particular, from Figure 1a and Figure 1b, it is clear that the variation of the orientation angle leads to a rotation of the filter response.

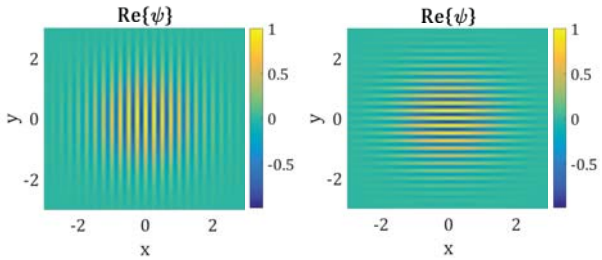

(a) $\theta = 0°$ (b) $\theta = 90°$

Figure 1: Real part of a Gabor filter response in the XY plane, with $\eta = \gamma = 2\pi$ and $f = 4$.

978-1-4799-7444-3/15 /$31.00 ©2015 IEEE

Figure 2, instead, represents the magnitude of the Gabor filter harmonic response in the UV plane, obtained from the responses in Figure 1. The harmonic response is a pulse whose position depends on both f and θ. Particularly, the pulse moves on a circumference centred in the origin and whose radius is defined by f, while θ is the rotation angle in the anti-clockwise direction with respect to the $\hat{u}$ axis, as shown in Figure 2a and Figure 2b. Hence, it is possible to extract local feature in the

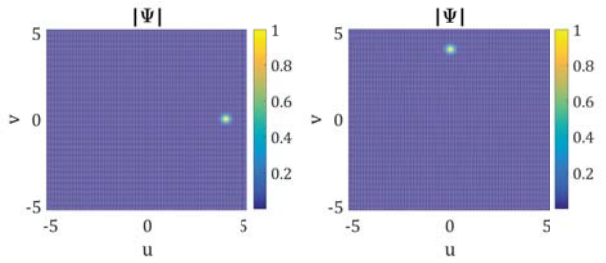

(a) $\theta = 0^\circ$ (b) $\theta = 90^\circ$

Figure 2: Magnitude of the Gabor filter harmonic response in the UV plane, with $\eta = \gamma = 2\pi$ and $f = 4$.

Fourier domain by varying the filter parameters.

In the following subsection the classification algorithm based on features extracted with the Gabor filters is presented.

III. Feature Extraction Algorithm

The principal aim of the algorithm presented in this paper is to extract features based on the micro-Doppler by using 2D Gabor filters. For this reason, a fundamental step is to obtain a 2D image from the received radar signal scattered by the target of interest. A block diagram of the algorithm is shown in Figure 3. The starting point of the algorithm is the received

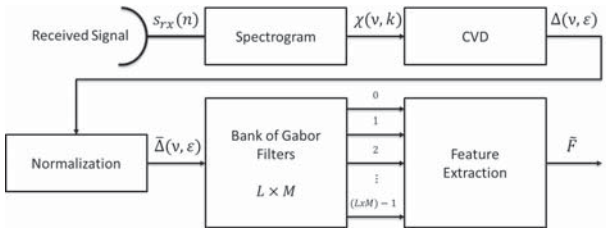

Figure 3: Block diagram of the proposed algorithm.

signal $s_{rx}(n)$, with $n = 0, ..., N-1$, containing the micro-Doppler components and where N is the number of signal samples. The first step is to evaluate the spectrogram through the computation of the modulus of the STFT (Short Time Fourier Transform) of the received signal $s_{rx}(n)$ as follows:

$$\chi(\nu,k) = \left| \sum_{n=0}^{N-1} s_{rx}(n) w_h(n-k) \exp\left(-j2\nu\frac{n}{N}\right) \right| \quad (5)$$
$$k = 0, \cdots, K-1$$

where ν is the normalized frequency and $w_h(.)$ is the smoothing window. The spectrogram is a time-frequency distribution that allows us to evaluate the signal frequency variation over the time and it is chosen for its robustness with respect to the interference terms present in other time-frequency distributions. The next step consists of extracting the CVD (Cadence Velocity Diagram), that is defined as the Fourier Transform of the spectrogram along each frequency bin [5] and is given by

$$\Delta(\nu,\varepsilon) = \left| \sum_{k=0}^{K-1} \chi(\nu,k) \exp\left(-j2\nu\frac{k}{K}\right) \right| \quad (6)$$

where ε is the cadence frequency. The choice of the CVD is motivated by the possibility of extracting useful information such as the cadence of each frequency component and the maximum Doppler shift. Moreover, the CVD is more robust than the spectrogram since it does not depend on the initial position of the moving object. Thereafter, the CVD is normalized in order to obtain a matrix whose values lie in the range $[0, 1]$ as follows

$$\bar{\Delta}(\nu,\varepsilon) = \frac{\Delta(\nu,\varepsilon) - \min\limits_{\nu,\varepsilon} \Delta(\nu,\varepsilon)}{\max\limits_{\nu,\varepsilon} \left[\Delta(\nu,\varepsilon) - \min\limits_{\nu,\varepsilon} \Delta(\nu,\varepsilon)\right]}. \quad (7)$$

Figure 4a and Figure 4b show an example of a normalized CVD and its 2D Fourier transform obtained from a signal scattered by a cylinder. Each element of the obtained matrix $\bar{\Delta}$

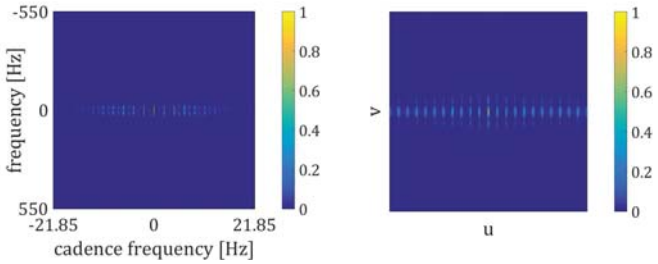

(a) CVD. (b) Transformed image.

Figure 4: Example of a normalized CVD and its 2-D Fourier transform obtained from a signal scattered by a cylinder.

is considered as a pixel of a 2D image and this image is given as input to a bank of Gabor filters whose responses change by varying the orientation angle and the central frequency, as in (1). The value of each pixel of the output image is given by the convolution product of the Gabor function and the input image, $\bar{\Delta}(\nu,\varepsilon)$, and may be written as follows

$$g_{l,m}(\nu,\varepsilon;f_l,\theta_m) = \psi_{l,m}(\nu,\varepsilon;f_l,\theta_m) * \bar{\Delta}(\nu,\varepsilon) = \quad (8)$$
$$\int_{-\infty}^{\infty}\int_{-\infty}^{\infty} \psi_{l,m}(\nu-\nu_\tau,\varepsilon-\varepsilon_\tau;f_l,\theta_m)\bar{\Delta}(\nu_\tau,\varepsilon_\tau)d\nu_\tau d\varepsilon_\tau$$

with $l = 0, \ldots, L-1$ and $m = 0, \ldots, M-1$, where L and M are the numbers of central frequencies and orientation angles, respectively. The principal aim of the variation of f_l and θ_m for each filter is to extract all the information contained in the CVD. Finally the output of the filters are processed to extract the feature vector used to classify the targets, which is the last step of proposed algorithm. In particular, a global feature is extracted from the output image of each filter by adding up the values of all the pixels, as follows

$$F_q = g_{l,m} = \sum_{\nu}\sum_{\varepsilon} |g_{l,m}(\nu,\varepsilon;f_l,\theta_m)| \quad (9)$$

where $q = mL+l$, with $l = 0, \ldots, L-1$, and $m = 0, \ldots, M-1$. Therefore, the obtained feature vector is given by

$$\boldsymbol{F} = \left[F_0\, F_1 \cdots F_{(L\times M)-1}\right]. \tag{10}$$

Finally it is normalised as follows:

$$\tilde{\boldsymbol{F}} = \frac{\boldsymbol{F} - \eta_{\boldsymbol{F}}}{\sigma_{\boldsymbol{F}}} \tag{11}$$

where $\eta_{\boldsymbol{F}}$ and $\sigma_{\boldsymbol{F}}$ are the statistical mean and the standard deviation of the vector $\boldsymbol{F}$, respectively.

The benefit of the use of the proposed algorithm is clearer in the Fourier domain where the filtering is given by the multiplication of the harmonic response of the 2D Gabor filter and the transformed input. As shown above, the harmonic response of the Gabor filter is a pulse whose position depends on f and θ. Since both the CVD and its 2D Fourier transform are characterized by vertical lines, as shown in Figure 4, the filter parameters can be tuned to match the lines, which are in different position for each class. This allows us to discriminate between different classes.

The classification performance of the extracted feature vectors is evaluated by using the k-Nearest Neighbour (k-NN) classifier, modified in order to account for the unknowns. Let $\mathcal{N}$ be the set of nearest neighbour training vectors for the feature vector $\mathbf{F}$, that is:

$$\mathcal{N} = \left\{\tilde{\mathbf{F}}_1, \ldots, \tilde{\mathbf{F}}_k : \min_{\tilde{\mathbf{F}}\in\mathcal{T}} \left\|\tilde{\mathbf{F}} - \mathbf{F}\right\|\right\} \tag{12}$$

where $\mathcal{T}$ is the training vectors set; moreover, let $\rho = [\rho_1, \ldots, \rho_k]$ be the labels of the vectors in $\mathcal{N}$, which can assume values in the range $[1, \ldots, V]$, where V is the number of possible classes. The unknown class is made in two steps. First each label $\rho_i, i = 1, \ldots, k$ is updated as follows:

$$\rho_i = \begin{cases} 0 & \tilde{\mathbf{F}}_i \notin \mathcal{S}_{\mathbf{CM}_{\rho_i}}(\zeta_{\rho_i}) \\ \rho_i & \text{otherwise} \end{cases} \tag{13}$$

where $\mathcal{S}_{\mathbf{CM}_v}(\zeta_v)$ is an hypersphere with centre $\mathbf{CM}_v$ and radius ζ_v, and $\mathbf{CM}_v$ is the centre of mass of the training vectors belonging to the class v. Secondly, let $\mathbf{s}$ be a $(V+1)$-dimensional score vector whose elements are the occurrences, normalised to k, of the integers $[0, \ldots, V]$ in the vector ρ; eventually, the estimation rule is implemented as follows:

$$\hat{v} = \begin{cases} \arg\max \mathbf{s} & \text{if} \quad \exists!(\max \mathbf{s}) > \frac{1}{2} \\ 0 & \text{otherwise} \end{cases} \tag{14}$$

where 0 is the unknown class.

Assuming that the feature vectors of each class are distributed uniformly around their mean vector, for all the analyses ζ_v is chosen equal to $\sigma_v\sqrt{12}/2$, where $\sigma_v = \mathrm{tr}(\mathbf{C}_v)$ and $\mathbf{C}_v$ is the covariance matrix of the training vectors which belong to the class v. The choice has been made according to the statistical proprieties of the uniform distribution. In fact, for an one dimensional uniform variable, the sum of the mean and the product between the standard deviation and the factor $\sqrt{12}/2$, gives the max possible value of distribution. Moreover, in order to consider the unknown class using a k-NN classifier, k has to be usually an integer greater than 1; then, k is set to 3. The choice of a k-NN classifier is justified for its low computational load and its capability of providing score values as an output. However, in general other classifiers with similar characteristics could also be selected.

IV. Experimental Results

In this section the effectiveness of the proposed algorithm is demonstrated using real data. The data has been realized using reproductions of the targets of interest. Particularly, two possible types of warhead have been considered, approximated by a simple cone and a cone with triangular fins at the base, while three are the possible decoys, approximated by a cylinder, a cone and a sphere.

According to the used model, the conical warhead has a diameter, d, of 1 m and a height, h, of about 0.75 m, while the fin's base, b_f, is 0.20 m and the height, h_f, is 0.50 m, as shown in Figure 5. The sizes of the decoys are usually

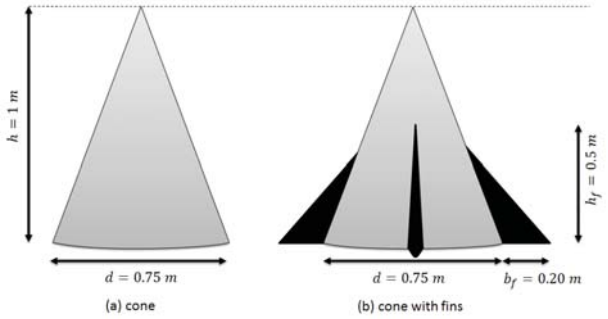

Figure 5: Model for two types of warhead.

comparable with the dimensions of the warheads in order to increase the number of false alarms. Therefore, according to the used model both the cylindrical and the conical decoys have diameter and height 0.75 m and 1 m respectively, while the sphere diameter is 1 m, as shown in Figure 6.

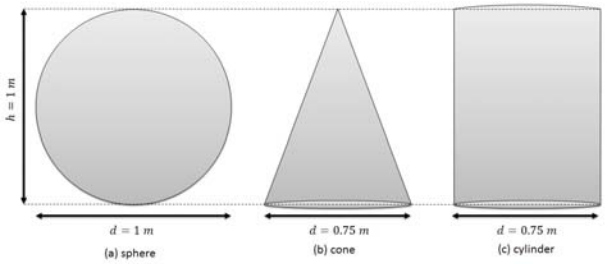

Figure 6: Model for three types of decoy.

The signals scattered by the replicas of the targets have been acquired by using a Continuous Wave (CW) radar, on varying the azimuth and the elevation angles. In particular, 10 acquisitions of 10 seconds have been made for each targets and for each possible couple of azimuth and elevation angles using three possible values for both of them, which are $[0°; 45°; 90°]$. The different movements of the warheads and the decoys have been simulated by using a ST robotic manipulator R-17 and an added rotor motor [13].

A. Results

In this section the proposed algorithm is compared with the Pseudo-Zernike (PZ) moments based feature vector approach,

presented in [5]. The targets of interest for the described analysis are divided in two classes which are *Warhead* and *Decoy*. Moreover, both of them are divided in sub-classes, and in particular the *Warhead* class comprises two sub-classes, one for warheads without the fins and the other one for those with fins, while *Decoy* class comprises three sub-classes each of them associated with one of the three different types of considered decoys.

In order to analyse the performance of the proposed algorithm, three figures of merit are considered which are the probabilities of *correct Classification* (P_C), *correct Recognition* (P_R) and *Unknown* (P_U). In particular, according to the following definition of probability

$$\frac{\#\text{ number of occurances}}{\#\text{ number of analysed cases}} \quad , \tag{15}$$

P_C is defined as the number of correct classified objects over the total number of analysed objects considering the two principal classes, while the second probability is calculated considering the classification on the five sub-classes; finally, the third figure of merit is given by the ratio of number of analysed objects for which the classifier does not take a decision and the total number of tests.

In order to statistically characterize the classifier and its performance, a Monte Carlo approach has been used, calculating the mean of the three figures of merit on several cases. In particular, 50 different runs have been carried out in which all the available signals have been divided randomly in 70% used for training and 30% for testing.

The spectrogram is computed by using a Hamming window with 75% overlap, and a varying number of points for the DFT, N_{bin}, which depends on both the used Hamming windows and the number of signal samples in order to obtain a square matrix for the spectrogram.

The algorithm is tested varying the observation time, which can be of 10, 5 and 2 seconds, the SNR and the dimension of the bank of filters, which depends on the chosen orientation angular pass θ_{step}. Specifically, the number of filters, Q, is given by

$$Q = L \times \left(\left\lceil \frac{\pi/2}{\theta_{step}} \right\rceil + 1 \right) \tag{16}$$

where $\lceil x \rceil$ is the ceiling function which gives the largest integer $\geq x$. The latter is fixed for the analysis, particularly 4 frequencies are used whose values are 0.5, 1, 1.5 and 2, while the integer values of θ_{step} varies in the interval $[3°, 10°]$.

Figure 7 shows P_C and P_R versus the dimension of the bank of Gabor filters for different signal's duration. Analysing the results, it is possible to note that the average correct classification is greater than 0.98 for any value of Q and for both the signal's duration of 10 and 5 seconds; classification performance slightly decreases for the 2 seconds observation time case, due to the reduced amount of micro-Doppler information contained in the analysed signal. Moreover, the performance has shown that P_U is always under 0.02 for all the values of both the number of filters and the signal's duration. Figure 8a shows the performance on varying the SNR and with $Q = 124$. In particular, assuming that the noise is negligible for the acquired signals, the analysis over the SNR has been conducted by adding white Gaussian noise. It is clear that P_C and P_R slightly decrease as the signal's duration decreases while they improve by increasing the SNR, especially they are

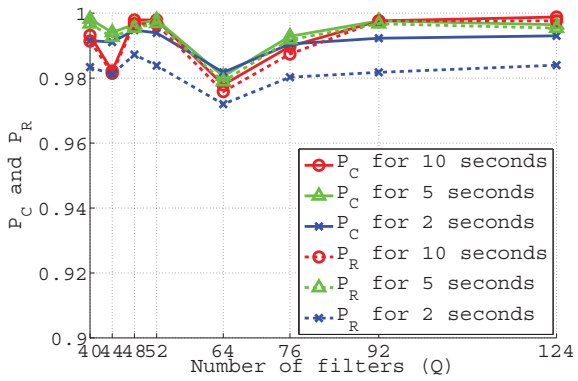

Figure 7: Probabilities of correct Classification, P_C, and correct Recognition, P_R, on varying Q and the duration of the observation.

greater than 0.99 when the SNR is above 0 dB. However, while for 10 seconds the performance remains almost constant, it decreases for signals of 5 and 2 seconds and for lower values of SNR. Figure 8b shows the performance of the PZ based algorithm for moments order of 10, which means that the length of the feature vector is $(order + 1)^2 = 121$. From the figure, it can be noted that for this algorithm the performance increases with the SNR. However, P_C and P_R are greater using the algorithm based on Gabor Filter for any value of SNR, when comparable dimensions of the feature vectors for the two approaches are considered.

Finally, Figure 9 represents P_U for both the algorithms when the SNR and the observation time are varied. As shown, while for the proposed method P_U is smaller than 0.01 in any analysed case, for the PZ features the performance improves by increasing both the signal's duration and SNR. P_U becomes smaller than 0.01 for any analysed observation time when the SNR is greater than 5 dB, however it is worse compared to the performance obtained with the Gabor features.

V. Conclusion

In this paper a novel algorithm used to extract robust feature based on micro-Doppler signature is presented. In particular, the algorithm takes advantage of the 2D Gabor filter applied on the normalized Cadence Velocity Diagram evaluated from the received signal. The reliability of the novel features has been demonstrated by testing them on real micro-Doppler data with the aim to classify between warheads and decoys. The performance has shown that these features generally ensure to correctly classify a ballistic target with a probability greater than 0.99 between different classes and, in particular, the performance is high also for low values of the SNR considering signals whose duration is bigger than 5 seconds. The proposed algorithm has been compared with the method which uses the Pseudo-Zernike moments based feature vector showing that the novel approach ensures better performance for the same number of features.

Acknowledgment

This work was supported by the Engineering and Physical Sciences Research Council (EPSRC) Grant number EP/K014307/1.

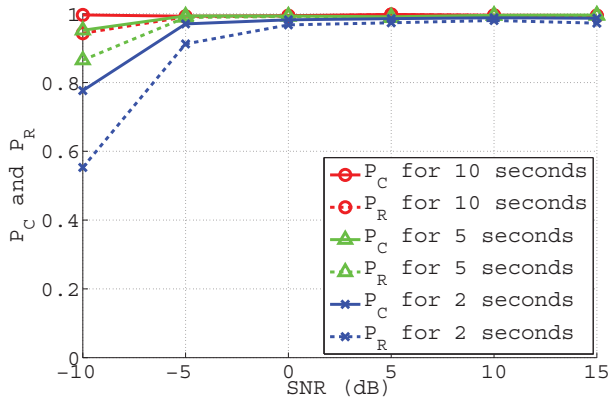

(a) Gabor features, $Q = 121$

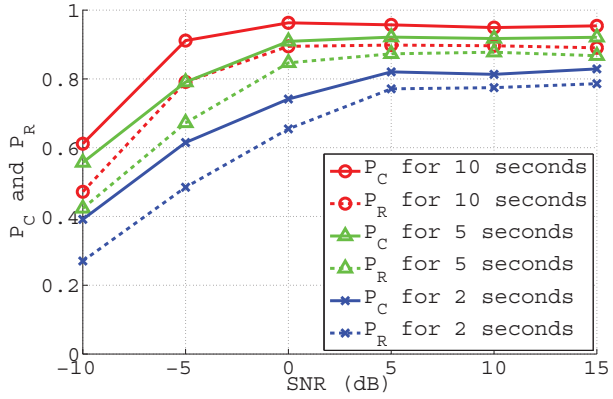

(b) PZ feature, order 10

Figure 8: Probabilities of correct Classification, P_C, and correct Recognition, P_R, on varying the SNR and the signal's duration.

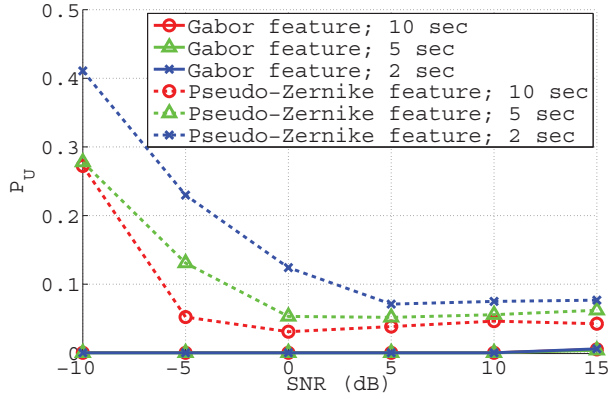

Figure 9: Unknown Probability, P_U, on varying the SNR and the signal's duration for the Gabor filter based and the Pseudo-Zernike moments based approaches.

REFERENCES

[1] V. Chen, F. Li, S. Ho, and H. Wechsler, "Micro-Doppler effect in radar: Phenomenon, model, and simulation study," *IEEE Transactions on Aerospace and Electronic Systems*, vol. 42, no. 1, pp. 2–21, Jan 2006.

[2] C. Clemente, A. Balleri, K. Woodbridge, and J. Soraghan, "Developments in target micro-Doppler signatures analysis: radar imaging, ultrasound and through-the-wall radar," *EURASIP Journal on Advances in Signal Processing*, vol. 2013, no. 1, 2013.

[3] L. Liu, D. McLernon, M. Ghogho, W. Hu, and J. Huang, "Ballistic missile detection via micro-Doppler frequency estimation from radar return." *Digital Signal Processing*, vol. 22, no. 1, pp. 87–95, 2012.

[4] G. Hongwei, X. Lianggui, W. Shuliang, and K. Yong, "Micro-Doppler signature extraction from ballistic target with micro-motions," *IEEE Transactions on Aerospace and Electronic Systems*, vol. 46, no. 4, pp. 1969–1982, Oct 2010.

[5] L. Pallotta, C. Clemente, A. De Maio, J. Soraghan, and A. Farina, "Pseudo-zernike moments based radar micro-doppler classification," in *Radar Conference, 2014 IEEE*, May 2014, pp. 0850–0854.

[6] C. Clemente, L. Pallotta, I. Proudler, A. De Maio, J. Soraghan, and A. Farina, "Pseudo-zernike-based multi-pass automatic target recognition from multi-channel synthetic aperture radar," *Radar, Sonar Navigation, IET*, vol. 9, no. 4, pp. 457–466, 2015.

[7] J.-K. Kamarainen, V. Kyrki, and H. Kalviainen, "Invariance properties of gabor filter-based features-overview and applications," *Image Processing, IEEE Transactions on*, vol. 15, no. 5, pp. 1088–1099, May 2006.

[8] J. Ilonen, J. Kämäräinen, and H. Kälviäinen, "Efficient computation of gabor."

[9] V. Kyrki, J.-K. Kamarainen, and H. Kälviäinen, "Simple gabor feature space for invariant object recognition," *Pattern recognition letters*, vol. 25, no. 3, pp. 311–318, 2004.

[10] N. Mittal, D. Mital, and K. L. Chan, "Features for texture segmentation using gabor filters," in *Image Processing And Its Applications, 1999. Seventh International Conference on (Conf. Publ. No. 465)*, vol. 1, Jul 1999, pp. 353–357 vol.1.

[11] J. Ilonen, J.-K. Kamarainen, and H. Kalviainen, "Fast extraction of multi-resolution gabor features," in *Image Analysis and Processing, 2007. ICIAP 2007. 14th International Conference on*, Sept 2007, pp. 481–486.

[12] J. Lei and C. Lu, "Target classification based on micro-doppler signatures," in *Radar Conference, 2005 IEEE International*, May 2005, pp. 179–183.

[13] S. A. P. Ltd., "Robotics within reach," Tech. Rep. [Online]. Available: http://www.strobots.com/images/Brochure.pdf